NISS

Parameter space of an ocean general circulation model using an isopycnal mixing parameterization

William A. Gough and William J. Welch

Technical Report Number 3
December, 1993

National Institute of Statistical Sciences
19 T. W. Alexander Drive
PO Box 14006
Research Triangle Park, NC 27709-4006
www.niss.org

Parameter space of an ocean general circulation model using an isopycnal mixing parameterization

William A. Gough[1]
Canadian Climate Centre
4905 Dufferin St.
Downsview, Ontario
M3H 5T4

William J. Welch
Department of Statistics and Actuarial Science
University of Waterloo
Waterloo, Ontario
N2L 3G1

[1] Current affiliation: Physical Sciences Division
Scarborough College, University of Toronto
1265 Military Trail
Scarborough, Ontario, M1C 1A4

Abstract

In this study we have employed statistical methods to efficiently design experiments and analyze output of an ocean general circulation model that uses an isopycnal mixing parameterization. Full ranges of seven inputs are explored using 51 numerical experiments. Fifteen of the cases fail to reach a satisfactory equilibria. These are attributable to numerical limitations specific to the isopycnal model. Statistical approximating functions are evaluated using the remaining cases to determine the dependency of each of the six scalar outputs on the inputs.

With the exception of one output, the approximating functions perform well. Known sensitivities, particularly the importance of diapycnal (vertical) diffusivity and wind stress, are reproduced. The sensitivities of the model to two numerical constraints specific to the isopycnal parameterization, maximum allowable isopycnal slope and horizontal background diffusivity, are explored. Isopycnal modelling issues, convection reduction and the Veronis effect, are examined and found to depend crucially on the isopycnal modelling constraints.

1. Introduction

The isopycnal version of the Bryan-Cox ocean general circulation model has been used by several investigators (Cummins et al., 1990; Gerdes et al., 1991; Gough, 1991; England, 1992; Manabe et al., 1991; Gough and Lin, 1992). A comprehensive examination of the parameter space of this model, though, has not been reported. The 'isopycnal' nature of the model refers to the method in which sub-grid scale processes are parameterized. Traditionally, (Bryan, 1969; Cox, 1984) these processes are aligned to the coordinate surfaces which are geopotentials and the perpendiculars to geopotentials (horizontal and vertical). It has been suggested in the literature that mixing processes would be better modelled along isopycnals (constant density surfaces) and diapycnals (perpendiculars to constant density surfaces) (Veronis, 1975; Sarmiento, 1983; McDougall and Church, 1986).

Montgomery (1940) and others suggested that large scale oceanic flow may mix preferentially along isopycnals. For example, it was noted from observational data that there were no salinity maxima on isopycnal surfaces, except at the intersections of these surfaces with the wind-driven mixed layer and lateral boundaries. Broecker and Peng (1982) examined the ^{3}He distributions in the Pacific, and found that this tracer appeared to spread along isopycnals into the other ocean basins.

Other evidence to support isopycnal mixing is less direct. It has been proposed to explain deficiencies in modelling studies. Veronis (1975) first noted the appearance of anomalous heat, and

therefore density fluxes near the western boundary in Holland's (1971) model simulation of the general circulation of the North Atlantic. He argued that lateral mixing in that reqion produced a large diapycnal flux. As the lateral boundaries are thermally insulated, this heat (or density perturbation) could only be balanced by an increase in the upwelling of cold water. This enhanced upwelling, in turn, needed to be compensated by increased downwelling elsewhere, as reflected in Holland's results. This is contrary to the classical view (Stommel, 1958) of weak, widespread upwelling in the ocean interior. Veronis further suggested that the use of an isopycnal mixing parameterization would eliminate this problem, as the removal of a large diapycnal flux in the western boundary would no longer result in enhanced upwelling. McDougall and Church (1986) also invoked isopycnal mixing to explain large density fluxes found in the same region in the results of Cox and Bryan (1984). Note that both Holland (1971) and Cox and Bryan (1984) used a large horizontal eddy diffusivity. Veronis (1975) reported that the use of a lower diffusivity mitigated the downwelling problem. Gough (1991) found that the 'Veronis effect' was lower for the isopycnal model. This reduction, though, was limited by a horizontal background diffusivity required for numerical stability. He also found that the isopycnal model produced a shallower thermocline, weaker thermohaline circulation, and a dramatic reduction in the number of convection points. This reduction appears to be only partially compensated by an increase in vertical diffusivity due to sloping isopycnals in convective

regions.

In this study the isopycnal model is examined over a broader range of parameter values than was used in Gough (1991). One goal is to cover this broader range of physically reasonable values in a computationally efficient manner. Statistical techniques are used both to design the experiments and evaluate the output. The basic idea is to build a statistical approximation for each output of interest (kinetic energy density, etc.) as a function of several inputs considered (diffusivities, etc.). Model sensitivities can then be quickly evaluated via the approximating functions, which are more computationally efficient to produce. In constrast, the ocean general circulation model is expensive to evaluate, so we construct the approximations using only a limited number of runs, chosen according to a statistical experimental design.

In Section 2 the model and experimental design are described. The methods for building the approximating functions, their use to estimate sensitivities, and the results are reported and discussed in Section 3. Finally, in Section 4 the conclusions are presented.

2. Model description and experimental design

2.1 Model

2.1.1 Governing equations

The model used in this work is the widely distributed Bryan-Cox ocean general circulation model. It is based on the pioneering work of Bryan (1969). A detailed description of the model can be found elsewhere (Cox, 1984). The notation used is standard and is listed in Appendix A.

Convection is treated differently here than it is in both Bryan (1969) and Cox (1984). They used an iterative approach in which successive layers were compared and temperature and salinity were homogenized when instabilities were found. In the present study, homogenization of temperature and salinity through intense vertical diffusion occurs when vertical instability is detected. Marotzke (1991) has found that this method effectively removes static instability. A value of $A_{DV} = 10^4$ cm^2/s is used for convective adjustment which is four orders of magnitude larger than the nominal vertical diffusivity value of $A_{DV} = 1$ cm^2/s (Killworth, 1989).

2.1.2 Boundary conditions

In this model the only source of heat (temperature) and salinity forcing is at the upper surface. Therefore, at the side walls and bottom, a no-flux condition is imposed.

For the vertical side walls there is a no-slip (u, v = 0) condition. At the bottom boundary, the flow is constrained to be parallel to the bottom topography, w = 0, in the case of this model with a flat bottom. The condition on u and v is determined by the imposed bottom friction,

$$(1) \quad \tau_\lambda = \rho_o C_D (u^2+v^2)\ (u\cos\alpha - v\sin\alpha)$$
$$(2) \quad \tau_\phi = \rho_o C_D (u^2+v^2)\ (u\sin\alpha - v\cos\alpha)$$

where C_D, the drag coefficient, is 1.3×10^{-3} and α, the turning angle, is -10° for this study. For the vertical velocity, the rigid lid approximation is used (w=0 at z=0).

The horizontal momentum, at the upper surface, is forced by the atmospheric winds. This is accomplished by using idealized wind stresses (τ_λ, τ_ϕ) given by the following analytic representation,

$$(3) \quad \tau_\phi = 0.2 - 0.8\sin(6\phi)$$
$$(4) \quad \tau_\lambda = 0.0$$

with the stress in units of dynes/cm^2. This particular choice is designed to give a two gyre circulation in the North Atlantic, the approximate region of the model domain.

In this work restoring boundary conditions are used for both temperature and salinity (Haney, 1971). Zonally and temporally averaged (annual mean) restoring temperatures (T^*) and salinities (S^*) are taken from the Levitus (1982) climatological atlas for the ocean. These values are presented in Fig. 1 with the implied restoring densities. The value of D, the diffusion constant, is 46.3 $Wm^{-2}{}^\circ C^{-1}$ and is taken as a constant, spatially and temporally; this corresponds to a restoring timescale of 50 days for a 50 m

upper layer.

2.1.3 Parameterization of sub-grid scale processes

In the momentum equation, the sub-grid scale processes are parameterized using eddy viscosities. Due to the predominantly horizontal flow, the horizontal eddy viscosity, $A_{MH} \equiv 10^9$ cm^2/s, which is much larger than the vertical eddy diffusivity, $A_{MV} \equiv 1.0$ cm^2/s. Bryan (1987) showed that there is much less sensitivity to the parameterization used in the momentum equations than there is in the temperature and salinity equations. In particular, Bryan found that the depth of the thermocline, the meridional and zonal mass transports, and the northward heat transport all depended crucially on the value chosen for the vertical eddy diffusivity.

As discussed in the Introduction the parameterization of the sub-grid scale eddy processes could be done using isopycnal and diapycnal mixing rather than the traditional vertical and horizontal (geopotential) coordinate system. Redi (1982) derived a coordinate transformation which represents isopycnal mixing in a model based on a geopotential coordinate system. Cox (1987) produced the necessary code to implement this mixing in the Bryan-Cox model.

Two assumptions are made to simplify the Redi tensor (Cox, 1987). Since mixing along isopycnals greatly exceeds mixing across isopycnals we assume that $\epsilon << 1$; the isopycnal slope is usually small $\delta < 10^{-2} << 1$. Here, $\epsilon = A_D/A_I$, the ratio of the diapycnal to isopycnal eddy diffusivity and $\delta = (\rho_x^2 + \rho_y^2)^{1/2}/\rho_z$. This results in

a simplified tensor,

$$(5)\quad \mathbf{K} = A_I \begin{vmatrix} 1 & \frac{-\rho_x\rho_y}{\rho_z^2} & -\frac{\rho_x}{\rho_z} \\ \frac{-\rho_x\rho_y}{\rho_z^2} & 1 & -\frac{\rho_y}{\rho_z} \\ -\frac{\rho_x}{\rho_z} & -\frac{\rho_y}{\rho_z} & \epsilon+\delta^2 \end{vmatrix}$$

The indices x, y and z denote the partial differentiation with respect to zonal, meridional and vertical directions respectively.

2.2 Inputs and Outputs

Seven input parameters are examined, the diapycnal and isopycnal eddy diffusivities (A_D, A_I), the vertical and horizontal eddy viscosities (A_{MV}, A_{MH}), the background eddy diffusivity (A_B), the maximum allowable slope (δ_m), and the peak value of the wind stress (τ_m).

The background eddy diffusivity and maximum allowable slope are numerical constraints arising from the use of the isopycnal mixing parameterization (Cox, 1987). The peak wind stress value is varied by changing the coefficient of the sine term in Eq. 3. Table 1 contains the range of values for the seven parameters. These ranges should be kept in mind when interpreting the results: sensitivity with respect to a parameter would tend to increase if a wider range is chosen.

The model flow is represented by six scalar outputs. They are the basin averaged kinetic energy density (KE), the peak value of the meridional streamfunction (MMT), the peak value of the

northward heat transport (NHT), the bottom temperature at 63° N, 30° W (TEMP), the number of convecting points (CONV) and the number of downwelling points (DOWN). The first three are familiar measures of the model flow. The bottom temperature at 63°N, 30°W is a measure of the deep water formation in the northern convective region. The number of convecting points was shown to substantially reduce with the use of an isopycnal mixing parameterization (Gough 1991). Enhanced vertical diffusivity due to the parameterization effectively replaced convection. The number of downwelling points is a measure of the Veronis effect (Veronis, 1975).

2.3 Experimental Design

A total of 51 experiments (Table 2) are performed to explore the parameter space defined by the ranges in Table 1. To insure the efficient use of computing resources statistical techniques are employed to design the experiments and evaluate the model output.

To sample the seven parameter input space uniformly, a Latin hypercube experimental design (McKay et al., 1979) is used. These designs were proposed for deterministic numerical experiments (i.e., without random error, as here).

To construct a Latin hypercube for n model runs, each parameter's range is represented by an equally-spaced grid of n values. Thus the range is fully explored. Available computer resources allow for an initial 25 to 30 runs of the model to be completed in a reasonable time (two weeks) on a series of workstations. Taking n = 26 runs gives spacing of 1/25 of each

parameter's range. Because the maximum allowable isopycnal slope has a range covering two orders of magnitude, we actually work with the logarithm of this parameter. Therefore, the $\log(\delta_m)$ values are equally spaced. Similarly, in subsequent statistical analysis we will work with $\log(\delta_m)$ rather than δ_m.

For a completely random Latin hypercube, the 26 values for a parameter are in random order. Therefore, we would have each individual parameter's range uniformly covered, and the random ordering leads to various combinations covering the multidimensional space. For greater control of the multidimensional properties, though, we modify a completely randomized arrangement. Iman and Conover (1982) described how to transform a random Latin hypercube into one with a desired correlation pattern of zero. Here, we are manipulating the input parameters independently of one another, and each pair of parameters should be uncorrelated. The method proposed by Iman and Conover does not generate a Latin hypercube with pairwise correlations. Very small correlations can be achieved, however, by iterating, an obvious adaptation of their method. In this way, the design in the first 26 rows of Table 2 has correlations less than 0.04 for all pairs of parameters, and the two dimensional properties of the design are controlled.

Of the 26 runs, five prove unstable (refer to Section 3.1). Following the method to be outlined in Section 3.2, approximating functions are fitted and assessed for accuracy for each output using the 21 successful runs. For now, though, we just note that these functions do not yield sufficient accuracy, and a further 25

model runs are made.

These additional runs are chosen to augment the 21 successful runs from the first experimental design. To improve the coverage of the input space, the 25 new runs are selected to fill in sparse subregions. Specifically, the new input points are chosen to be distant from the successful first-stage design points and from each other. These additional runs are given in rows 27-51 of Table 2.

Of the 25 new runs, 10 are unstable. The 15 successful runs, together with the 21 from the first-stage design, give a total of 36 stable cases. All output data appear in Table 3.

3. Results and Discussion

The 51 experiments are integrated for 1500 years. The integrations are begun at rest. A split time step method is used (Bryan, 1984); the temperature and salinity equations use a one day time step whereas the momentum equations use a 30 minute time step. Due to the restoring density field (Fig. 1) a density driven (thermohaline) circulation is set up. There is intense downwelling in the north where the restoring density peaks and gradual upwelling in much of the rest of the domain. A wind driven Ekman circulation is also generated in the upper ocean. The strength of this circulation is dependent on the magnitude of the peak wind stress.

The results are divided into four sections. The first is an examination of the cases that did not achieve a stable solution after 1500 years. In the second section the performance of a statistical model of the ocean general circulation model based on the model output is presented. In the third section, the dependence of output scalars on the input parameters is explored using the statistical model. Finally, in the fourth section, an overall assessment of the input parameters is made.

3.1 Unstable cases

Fifteen of the 51 cases are considered unstable. Cases 3, 15, 18, 19, 27, 29, 31, 36, 38, and 46 exhibit explosive behaviour and the integrations are terminated. Cases 23, 34, 42, and 48 have

unconverged, oscillatory solutions by year 1500. Finally, 'negative diffusion' resulting in bottom water that is colder than the coldest restoring temperature has been detected in case 39 similar to that found by Gough (1991) and Gerdes et al. (1991). Negative diffusion is also detected in oscillatory cases 34 and 48, and unstable case 3.

Nine of the unstable cases can be attributed to a numerical constraint associated with the use of the isopyncal mixing parameterization. Cox (1987) derived the following constraint on the maximum allowable slope,

$$(6)\quad \delta_m < \left(\frac{\Delta a \Delta z}{4 A_I \Delta t}\right)^{1/2}$$

where Δa, Δz, Δt, and A_I refer to the horizontal grid spacing, vertical grid spacing, timestep, and isopycnal diffusivity, respectively. Choosing the smallest horizontal grid spacing (at the most northerly latitudes) and smallest vertical level depth, it is found that the maximum allowable slopes selected for cases 15, 18, 19, 27, 29, 31, 36, 38, and 46 do not satisfy this criteria, all of which displayed explosive behaviour.

The remaining unstable cases are characterized by a low background diffusivity (cases 3, 34, and 48) or low combined background and isopycnal diffusivity (cases 23 and 42). Cox (1987) indicated that it may be necessary to include a background diffusivity to suppress the growth of a computational mode. Case 30 which was stable had a background diffusivity of 1.03×10^7 cm^2/s, less than that of case 34. The stability of this case, though, is

likely the result of the very shallow maximum allowable isopycnal slope (0.001, an order of magnitude smaller than cases 3, 34, and 48), and a sufficiently large isopycnal diffusivity (1.576 x 10^7 cm^2/s). Bryan et al. (1975) reported that the horizontal diffusivity needed to be sufficiently large to suppress the computational mode which may explain the behaviour of cases 23 and 42. Theirs is the lowest combined values of the background and isopycnal diffusivity.

The 'negative diffusion' found in cases 3, 34, 39, and 48 is associated with three input parameters; large isopycnal diffusivity, low background diffusivity, and steep maximum isopycnal slope. Other cases with a large isopycnal to background diffusivity ratio which do not produce negative diffusion have a shallow maximum isopycnal slope (eg. cases 10, 30, and 51). Gerdes et al. (1991) attributed the negative diffusion to the use of one-sided differences at boundaries in regions that were topographically isolated from advection. A definitive threshold for negative diffusion as a function of these three inputs has not been obtained from the results.

3.2 Statistical Modelling

Using the 36 stable cases listed in Table 3, statistical approximating functions are constructed for each output as a function of the seven inputs. We follow the methodology described in Sacks et al. (1989a); Sacks et al. (1989b); and Welch et al. (1992). Bowman et al. (1992) applied these methods to an

atmospheric model. Details can be found in these papers; here we outline the main ideas.

Let $\mathbf{x} = (x_1,\ldots,x_7)$ denote the vector of input parameters, and let y denote one of the outputs (each of the six outputs of interest is dealt with in turn). We treat $y(\mathbf{x})$ as a realization of a stochastic process,

$$(7) \quad Y(\mathbf{x}) = \beta_0 + Z(\mathbf{x})$$

where β_0 is an unknown constant and $Z(\mathbf{x})$ is a random function with mean zero and correlation function $R(\mathbf{w},\mathbf{x})$ between the two Z values at input $\mathbf{w}$ and $\mathbf{x}$. Note that a realization of a stochastic process is non-random, like the deterministic computer model here, but embedding the function in a stochastic structure gives a basis for constructing a predictor.

Central to this model is the correlation function $R(\mathbf{w},\mathbf{x})$. Sacks et al. (1989b) found,

$$(8) \quad R(\mathbf{w},\mathbf{x}) = \Pi_j e^{(-\theta_j|w_j-x_j|^{p_j})}$$

to be useful in a number of applications, where $\theta_j \geq 0$ and $0 < p_j \leq 2$ are parameters to be estimated. If we further assume that the stochastic process in Eq. 7 is Gaussian, the optimization of these parameters by maximum likelihood to tune the model to the data is straightforward. Qualitatively, this correlation structure implies that two input vectors $\mathbf{w}$ and $\mathbf{x}$ are close together in the input space should give rise to values of the output function that are highly correlated (i.e., similar), as would be expected if the function is smooth. Conversely, $\mathbf{w}$ and $\mathbf{x}$ when remote from each other

lead to two output values with low correlation (i.e., unrelated).

Thus, we first tune the statistical model to the data: β_o in Eq. 7, $\theta_1,\ldots,,\theta_7$ in Eq. 8, and $p_1,\ldots,p_7$ in Eq. 8 are estimated by maximum likelihood. Then, a best linear unbiased predictor,

$$(9)\quad \hat{y}(\boldsymbol{x}) = \beta_o + \boldsymbol{r}'(\boldsymbol{x})\ \boldsymbol{R}_D^{-1}\ (\boldsymbol{y}-\beta_o\mathbf{1})$$

is compute4d where r(x) is an n X 1 vector of correlations with element i given by $R(\mathbf{d}_i,\mathbf{x})$ in Eq. 8 and $\mathbf{d}_i$ is the vector of input parameters for run i of the numerical model; $\mathbf{R}_D$ is an n x n matrix of correlations with elements i,j given by $R(\mathbf{d}_i,\mathbf{d}_j)$ in Eq. 8; **1** denotes an n x 1 vectors of 1's; **y** is the n x 1 vector of output values from the numerical model for a particular response; and β_0 is the generalized least squares estimator of β_0 given by $\beta_0 = \mathbf{1'R_D\ y/\ 1'R_{D-1}\ 1}$. This predictor is more flexible than, say, a low-order polynomial fit, and has been found to yield more accurate predictions in various applications.

To assess the fidelity of the statistical model, predicted values using the tuned model are plotted against the actual model output in Fig. 2. The ith value if the response, y_i is predicted using all data except y_i, a method of prediction-accuracy assessment known as cross validation. There is reasonable agreement between predicted and actual values for the first five outputs. In Fig. 2a for the large values of kinetic energy the statistical model under predicts the value. Similarly large values of convection are not as well predicted as lower values are. The overturning streamfunction, the northward heat transport, and the bottom temperature are all well predicted. In Figure 2f, the

modelling of downwelling points is seen to be less accurate, however, and for this output our results should be treated with caution. This means the ocean general circulation model is reasonably predictable, and our subsequent results and inferences about sensitivities appear to be based on reliable approximations.

3.3 Dependencies of Output on Input

The predictor, Eq. 9, "explains" the dependency of an output y on multi-dimensional inputs x_1, ..., x_7. To assess sensitivities, however, we want to determine the effect of individual x variables on y. To estimate the effect of x_j integrate out all other inputs from y:

$$(10)\quad \hat{\mu}_j(x_j) = \frac{\int \hat{y}(x_1, \ldots, x_7)\, \Pi_{i*j} dx_i}{\Pi_{i*j}(b_i - a_i)}$$

where (a_i, b_i) is the range of values for x_i.

Similarly, the dependence on the joint effect of x_j and x_k can be estimated by integrating out all variables except these two,

$$(11)\quad \hat{\mu}_{jk}(x_j, x_k) = \frac{\int \hat{y}(x_1, \ldots, x_7)\, \Pi_{i*j,k} dx_i}{\Pi_{i*j,k}(b_i - a_i)}$$

and so on for higher order effects. To assess the importance of the joint effect over and above that explained by $\mu_j(x_j)$ and $\mu_k(x_k)$ we consider the estimated interaction effect,

$$(12)\quad \hat{\mu}_{jk}(x_j, x_k) - \hat{\mu}_j(x_j) - \hat{\mu}_k(x_k) + \hat{\mu}_o$$

where

$$(13)\quad \mu_0 = \frac{\int \hat{y}(x_1, \ldots, x_7) \prod_{i=1}^{7} dx_i}{\prod_{i=1}^{7} (b_i - a_i)}$$

is the overall estimated average value of the response y. If this interaction effect is small, x_j and x_k have approximately additive effects, it is sufficient to look at the separate $\mu_j(x_j)$ and $\mu_k(x_k)$ effects, and $\mu_{jk}(x_j, x_k)$ need not be inspected. This turns out to be the case for all outputs except convection (CONV). If a $\mu_{jk}(x_j, x_k)$ term is important, however, then it is difficult to isolate the effects of x_j or x_k individually, and we have to assess sensitivity with respect to both parameters jointly.

3.3.1 Kinetic energy density

Figure 3 shows the 'main effects', $\mu_j(x_j)$ plotted against x_j for the x variables estimated to have important effects on KE. Thus, the plot labelled KE (DIA) gives the estimated effect of diapycnal diffusivity on the kinetic energy. Unimportant x variables just give fairly horizontal plots; hence their omission.

Four factors are identified as important in determining the kinetic energy. Kinetic energy increases with diapycnal diffusivity and peak wind (WIND). It decreases with horizontal eddy viscosity (HORVIS) and background eddy diffusivity (BACK). The percentages attached to each plot give a quantitative assessment of the relative sensitivities. For example, of the total variability in kinetic energy due to varying all seven inputs over the ranges

investigated, peak wind alone accounts for an estimated 44.4%.

These dependencies are as expected and illustrate the two main circulations, wind driven (Ekman) and buoyancy driven (thermohaline). Bryan (1987) found that increasing the vertical diffusivity (the equivalent to the diapycnal diffusivity) increased the overturning streamfunction, a measure of the thermohaline circulation. Increasing the peak wind stress increases the Ekman circulation, thereby increasing the kinetic energy. Both the background eddy diffusivity and the horizontal eddy viscosity act to dampen the flow (particularly the gyre component) and thus cause a reduction in the kinetic energy. The horizontal eddy diffusivity acts directly on the flow whereas the background eddy diffusivity mixes temperature and salinity along horizontal surfaces causing diapycnal flow which smooths the density field. This results, through geostrophy, to a lower kinetic energy.

3.3.2 Meridional overturning streamfunction

There is one dominant component and one component of secondary importance in determining the peak value of the overturning streamfunction (MMT) (Fig. 4). As noted above this value is a measure of the buoyancy driven thermohaline circulation. The dominant effect is the increase of the streamfunction with the diapycnal diffusivity, a result consistent with Bryan (1987). The estimated increase of the overturning streamfunction with background diffusivity is marginal (only 3.7% of the total variability) and may be spurious. It should also be noted that the

surface buoyancy forcing which has remained constant for these experiments plays a major role in determining the nature and strength of the overturning streamfunction (Bryan, 1987).

3.3.3 Northward heat transport

The northward heat transport is known to depend upon both the buoyancy and wind driven circulations. From Fig. 5 we see that the heat transport depends strongly on the diapycnal diffusivity (98.2%). As noted in the previous section, increased diapycnal diffusivity increases the overturning streamfunction of the thermohaline circulation which results in a stronger heat transport. The increase of the peak wind intensifies the wind driven Ekman circulation also resulting in a stronger northward heat transport but this effect appears to be marginal (2.7% of the total variability).

3.3.4 Convection

There are two important inputs for the number of convection points: maximum isopycnal slope (72.2%) and isopycnal diffusivity (10.3%) (Fig. 6), with background diffusivity having a marginal effect (2.6%). For this output, however, we look to higher order effects: the $\mu_{jk}(x_j,x_k)$ term for the joint effect of maximum isopycnal slope (MAXSLP) and diapycnal diffusivity accounts for approximately another 8% of the variability and the joint effect of maximum isopycnal slope and isopycnal diffusivity accounts for another 3% in the number of convection points over and above the

separate effects.

The maximum isopycnal slope dependency is explainable in terms of cross isopycnal mixing. With a low maximum allowable slope, mixing is constrained to slopes less than the actual slope. This increases the diapycnal (cross isopycnal) flow and induces convection (Gough, 1991). As the maximum slope increases there is less diapycnal flux and, hence, less convection.

These results indicate that increasing the isopycnal diffusivity also reduces the number of convection points. By increasing the isopycnal diffusivity, temperature and salinity are more rapidly homogenized along isopycnals, thus reducing the potential for instability.

3.3.5 Bottom Temperature

There are four inputs that are important in the determination of the bottom temperature (Fig. 7). These are the diapycnal diffusivity (68.7%), the background diffusivity (15.8%), the peak wind stress (7.3%), and the peak wind (4.5%).

The source of cold bottom water is in the northern part of the domain through the surface restoring boundary condition on temperature. Water mass is transported via both the thermohaline and Ekman circulations to the bottom. If this combined circulation is intense then the downwelling waters are not cooled at the surface as much as those in a weaker flow. This mechanism explains the warmer temperature with increasing diapycnal diffusivity. As noted above the overturning streamfunction, and hence the

thermohaline circulation has a strong positive dependence on the diapycnal diffusivity. The dependence on the peak wind is similarly explained as the Ekman circulation intensifies with increasing peak wind.

The warming of bottom waters due to increasing background diffusivity is likely the result of the 'smoothing' effect of increased diffusivity. The bottom water at this location is typically the coldest water in the bottom of the basin. With increased horizontal diffusivity there is a mitigation of temperature gradients producing muted extremes.

The dependency on the maximum allowable slope probably results from the location of the coldest bottom temperature. Low isopycnal slope due to the shallower sloping of the isopycnals (Gough, 1991) produces a cold extreme further south than for higher slopes. Since the bottom temperature is taken at one location, the values are warmer for the shallower slopes. This affect, though, appears to be marginal.

3.3.6 Downwelling

As the statistical approximating function is not as good for this output as it was for the previous five outputs, the statistical inferences need to treated with care.

The dominant effects are identified as background diffusivity (59.8%), maximum isopycnal slope (13.1%), and diapycnal diffusivity (3.1%). The oscillatory nature of the diapycnal diffusivity is unlikely to be correct and should be discounted. The dependencies

upon the background diffusivity and the maximum isopycnal slope, though, are consistent with what is expected from the Veronis effect. As the background diffusivity is increased there is more cross isopycnal flow in the western boundary. This causes stronger upwelling there; hence an increase in the number of interior downwelling points. Increasing the maximum allowable slope reduces the cross isopycnal flow and thus there is a corresponding reduction in downwelling points.

3.4 Importance of inputs

This analysis has isolated the inputs which have the greatest impact on the selected model outputs. It is found that diapycnal diffusivity plays an important role for the kinetic energy, meridional overturning streamfunction, the northward heat transport, and the bottom temperature. These are expected from the results of Bryan (1987) where vertical diffusivity (his model's equivalent to diapycnal diffusivity) was found to play a pivotal role. Isopycnal diffusivity, in constrast, plays only a minor role in determining the number of convective points.

The importance of the peak wind stress on the kinetic energy, the northward heat transport, and bottom temperature is the result of a changed wind driven Ekman circulation, and is not surprising.

The horizontal eddy viscosity is important only for the kinetic energy where it acts to dampen the flow. This dampening affects the gyre (non zonal) component of the flow (Gough, 1991). The vertical eddy viscosity does not play a significant role for

any of the outputs. The value of this parameter is large enough for all experiments to prevent a Reynold's number violation (Weaver and Sarachik, 1990).

The maximum allowable slope is an important input for three of the outputs, convection, bottom temperature, and number of downwelling points. It, along with the isopycnal diffusivity, is crucial for the explanation of most of the unstable (explosive) cases detailed earlier (Sect. 3.1). It was noted in Gough (1991) that isopycnal mixing dramatically reduces the amount of convection. The maximum allowable slope can be taken as a measure of how 'isopycnal' the model is; the strong dependence of the convection on the maximum slope confirms the earlier work.

The other additional parameter, the required background horizontal diffusivity, is also shown to have important consequences. It plays a significant role in the kinetic energy, the bottom temperature, and the number of downwelling points. Low values of this parameter are identified with explosive or oscillatory behaviour in the experiments.

4. Conclusions

In this work we have shown that with the use of statistical techniques we have efficiently designed experiments to explore a wide range of the parameter space of the isopycnal version of the Bryan-Cox ocean general circulation model. Seven inputs are varied in 51 experiments. Fifteen of these cases are removed from the analysis due to explosive or oscillatory behaviour and 'negative diffusion'. The explosive behaviour is attributed to a numerical constraint violation for all but one of the explosive cases. Two of the oscillatory cases are the result of a combined low isopycnal and background diffusivity. The remaining cases have a large isopycnal to background diffusivity ratio resulting in 'negative diffusion' as identified in Gerdes et al. (1991).

In the analysis of the results six scalar outputs are used to characterize the flow. Statistical approximating functions of the ocean model is formed using the output. These functions, with one exception, show that the scalar output of the ocean general circulation model to be predictable. From this an analysis of the dependency of output on input is possible. Known sensitivities, such as the importance of the diapycnal diffusivity and peak wind stress, are reproduced. The impact of two new constraints, introduced for the isopycnal mixing parameterization, background diffusivity and the maximum isopycnal slope, is shown. Several inputs, the vertical and horizontal eddy viscosity and isopycnal diffusivity, play relatively minor roles for the ranges chosen for

these experiments.

Two isopycnal modelling issues are explored by the convection and downwelling outputs. Gough (1991) found that isopycnal mixing dramatically reduced convective activity compared to a similar lateral mixing model. These results are confirmed in this study. The more 'isopycnal' the model (large maximum allowable slope, low background diffusivity) the lower the number of convective points. The number of downwelling points is introduced as a measure of the Veronis effect. Although the approximating function is not as good as those for the other outputs the dependency on the two 'isopycnal' constraints, maximum allowable slope and horizontal background diffusivity are as expected, i.e. the more 'isopycnal' the model the fewer the number of downwelling points.

There are several applications for this type of model design and statistical modelling. First, this methodology provides an efficient manner to design a series of experiments to explore the parameter range of a model with a number of tunable inputs. The isolation of the more sensitive inputs can be used in further experimental design as well as testing of various different parameterizations. Input parameters can also be tuned to produce a known result, such as specific values for the northward heat transport or meridional overturning streamfunction. The methodology can also be expanded for use with vector inputs and outputs.

Another application is the production of output scalars for a given set of input parameters without actually running the full ocean general circulation model. This has application in simpler

climate modelling where computing resources may be limited.

In this set of experiments the equilibrium response to variation of inputs is examined. Another aspect of interest, particularly in climate change modelling, is the sensitivity of inputs on the transient response of a model.

Acknowledgments

We would like to acknowledge the helpful comments of C. Lin, K. Dixon, R. Gerdes, A. Weaver, T. Hughes, and F. Zwiers. The work was done while the first author was a Visiting Fellow at the Canadian Climate Centre of Environment Canada in Downsview, Ontario, Canada. WJW was supported by NSERC of Canada, AFOSR and NSF through Grant NSF-DMS-9121554. Part of the work was done while WJW visited the National Institute of Statistical Sciences.

Figure Captions

Fig. 1. Surface restoring values of a) temperature, b) salinity, and c) density. The temperature is in units of Celsius, the salinity in parts per thousand, and the density in sigma representation ($\sigma = \rho - 1000.0$ kg/m^3).

Fig. 2. Cross validation predictions for the six outputs.

Fig. 3. Kinetic energy density (KE) main effects, a) diapycnal diffusivity (DIA), b) horizontal eddy viscosity (HORVIS), c) horizontal background diffusivity (BACK), and d) peak wind stress (WIND).

Fig. 4. Meridional overturning streamfunction (MMT) main effects, a) diapycnal diffusivity (DIA), and b) horizontal background diffusivity (BACK).

Fig. 5. Northward heat transport (NHT) main effects, a) diapycnal diffusivity (DIA), and b) peak wind stress (WIND).

Fig. 6. Convection (CONV) main effects, a) isopycnal

diffusivity (ISO), b) horizontal background diffusivity (BACK), and c) maximum allowable isopycnal slope (MAXSLP).

Fig. 7. Bottom temperature (TEMP) main effects, a) diapycnal diffusivity (DIA), b) horizontal background diffusivity (BACK), c) maximum allowable isopycnal slope (MAXSLP), and d) peak wind stress (WIND).

Fig. 8. Downwelling (DOWN) main effects a) diapycnal diffusivity (DIA), b) horizontal background diffusivity (BACK), and c) maximum allowable isopycnal slope (MAXSLP).

Appendix A

α - Turning angle used in bottom drag

A_B - Background horizontal eddy diffusivity

A_D - Diapycnal eddy diffusivity

A_{MH} - Horizontal eddy diffusivity

A_{MV} - Vertical eddy diffusivity

C_D - Drag coefficient

δ - Isopycnal slope

δ_m - Maximum allowable slope

D - Diffusion constant

ϕ - Latitude

λ - Longitude

ρ - Sea-water density

S^* - Restoring salinity

τ_λ - Wind stress

τ_ϕ - Wind stress

T^* - Restoring temperature

T^S - Sea-surface temperature

u - zonal velocity

v - meridional velocity

w - vertical velocity

BACK - horizontal background diffusivity

DIA - diapycnal diffusivity

DOWN - number of downwelling points

HORVIS - horizontal eddy diffusivity

ISO - isopycnal diffusivity

KE - kinetic energy density

MAXSLP - maximum allowable slope

MMT - meridional overturning streamfunction

NHT - northward heat transport

TEMP - bottom temperature at 63°N, 30°W

VERTVIS - vertical eddy viscosity

WIND - peak value of the wind stress

References

Broecker, W. and T.-H. Peng, 1982: Tracers in the Sea. Lamont-Doherty Geological Observatory Publication (Palisades, New York).

Bowman, K.P., Sacks, J., and Y.-F. Chang, 1992: On the design and analysis of numerical experiments. J. Atmos. Sci. (in press).

Bryan, F., 1987: Parameter sensitivity of primitive equation ocean general circulation models. J. Phys. Oceanogr., 17, 970-985.

Bryan, K., 1969: A numerical method for the study of the circulation of the world ocean. J. Comput. Phys., 4, 347-376.

_____, Manabe, S. and R. Pacanowski, 1975: A global ocean-atmosphere climate model. Part II. The oceanic circulation. J. Phys. Oceanogr., 5, 30-45.

_____, 1984: Accelerating convergence to equilibrium of ocean-climate models. J. Phys. Oceanogr., 14, 666-673.

Cox, M., 1984: A primitive equation, three dimensional model of the ocean. GFDL Ocean Tech. Report No. 1, Princeton, NJ.

_____, 1987: Isopycnal diffusion in a z-coordinate ocean model. Ocean Modelling, 74, 1-5.

_____, and K. Bryan, 1984: A numerical model of the ventilated thermocline. J. Phys. Oceanogr., 14, 674-687.

Cummins, P., Holloway, G., and A. Gargett, 1990: Sensitivity of the GFDL ocean general circulation model to a parameterization of vertical diffusivity. J. Phys. Oceanogr., 20, 817-830.

England, M. E., 1992: On the formation of Antarctic intermediate and bottom water in ocean general circulation models. J. Phys. Oceanogr., 22, 918-926.

Gerdes, R., Koberle, C., and J. Willebrand, 1991: The influence of numerical advection schemes on the results of ocean general circulation models. Clim. Dyn., 5, 211-226.

Gough, W. A., 1991: Lateral and isopycnal mixing of passive and active tracers in an ocean general circulation model.

Ph.D. thesis. McGill University, Montreal, Canada. 147 pp.

_____ and C. A. Lin, 1992: The response of an ocean general circulation model to long time-scale surface temperature anomalies. Atmos.-Ocean, 30, 653-674.

Haney, R. L., 1971: Surface thermal boundary conditions for ocean circulation models. J. Phys. Oceanogr., 1, 241-248.

Holland, W., 1971: Ocean tracer distributions - a preliminary numerical experiment. Tellus, 23, 371-392.

Iman, R. L. and W. J. Conover (1982): A distribution-free approach to inducing rank correlation among input variables. Communications in Statistics B, Simulation and Computation, 11, 311-334.

Killworth, P.D., 1989: On the parameterization of deep convection in ocean models, in Parameterization of Small-Scale Processes, editted by P. Muller and D. Henderson, pp. 55-74, Hawaii Institute of Geophysics Special Publication, University of Hawaii.

Levitus, S., 1982: Climatological atlas of the world oceans. NOAA Prof. Paper 13, Washington, D.C.

Manabe, S., Stouffer, R., Spelman, M. and K. Bryan, 1991: Transient response of a couple ocean-atmosphere model to gradual changes of atmospheric CO_2. Part 1. Annual mean response. J. Clim., 4, 785-818.

Marotzke, J., 1991: Influence of convective adjustment on the stability of the thermohaline circulation. J. Phys. Oceanogr., 21, 903-907.

McDougall, T. and J. Church, 1986: Pitfalls with the numerical representation of isopycnal and diapycnal mixing. J. Phys. Oceanogr., 16, 196-199.

McKay, M. D., Conover, W. J., and R. J. Beckman, 1979: A comparison of three methods for selecting values of input variables in the analysis of output from a computer code, Technometrics, 21, 239-245.

Montgomery, R. 1940: The present evidence on the importance of lateral mixing processes in the ocean. Bull. Amer. Met. Soc., 21, 87-94.

Redi, M., 1982: Oceanic isopycnal mixing by coordinate rotation. J. Phys. Oceanogr., 12, 1154-1158.

Sacks, J., Schiller, S.B., and W. J. Welch, 1989: Designs for

computer experiments. Technometrics, 31, 41-47.

_____, Welch, W. J., Mitchell, T. J., and H. P. Wynn, 1989: Design and analysis of computer experiments (with discussion), Statistical Science, 4, 409-435.

Sarmiento, J., 1983: A simulation of bomb tritium entry into the Atlantic Ocean. J. Phys. Oceanogr., 13, 1924-1939.

Stommel, H., 1958: The abyssal circulation. Deep-Sea Res., 5, 80-82.

Veronis, G., 1975: The role of models in tracer studies. In Numerical models of ocean circulations. National Academy of Science. pp. 133-146.

Weaver, A. J. and E. S. Sarachik, 1990: On the importance of vertical resolution in certain ocean general circulation models. J. Phys. Oceanogr., 20, 600-609.

Welch, W. J., Buck, R. J., Sacks, J., Wynn, H. P., Mitchell, T. J., and M. D. Morris, 1992: Screening, predicting, band computer experiments, Technometrics, 34, 15-25.

Parameter	Range
Diapycnal eddy diffusivity, A_D	0.5 - 10.0 cm^2/s
Isopycnal eddy diffusivity, A_I	(0.5 - 5.0) x 10^7 cm^2/s
Vertical eddy viscosity, A_{MV}	0.5 - 20.0 cm^2/s
Horizontal eddy viscosity, A_{MV}	(0.5 - 3.0) x 10^9 cm^2/s
Background eddy diffusivity, A_B	(0.1 - 2.0) x 10^7 cm^2/s
Maximum allowable slope, δ_m	0.001 - 0.1
Peak wind stress, τ_m	0.0 - 1.8 dynes/cm^2/s

Table 1. Input parameter range

Case	A_D cm^2/s	A_I $10^7 cm^2/s$	A_{MV} cm^2/s	A_{MH} $10^9 cm^2/s$	A_B $10^7 cm^2/s$	δ_m	τ_m dynes/cm^2/s
1	0.500	1.400	17.66	0.700	2.000	0.0692	1.080
2	6.960	2.840	9.080	1.400	1.696	0.0331	1.800
3	5.440	3.380	16.10	1.100	0.100	0.0158	0.576
4	9.620	1.760	5.960	2.700	0.556	0.0052	0.216
5	0.880	5.000	12.20	1.300	0.860	0.0010	1.224
6	6.580	1.040	2.840	1.700	1.240	0.0063	0.504
7	4.300	4.100	19.22	1.900	1.392	0.0275	0.000
8	2.020	3.020	5.180	2.200	0.708	0.0479	0.792
9	2.400	0.860	9.860	1.000	0.252	0.0132	1.296
10	6.200	4.280	12.98	0.500	0.176	0.0025	0.144
11	2.780	1.580	4.400	2.400	0.784	0.0044	1.368
12	7.720	4.460	10.64	3.000	1.088	0.0036	1.728
13	1.640	3.560	11.42	2.900	1.924	0.0021	1.008
14	8.860	1.220	13.76	1.500	1.848	0.0110	1.152
15	9.240	4.640	2.060	1.600	1.316	0.0575	0.432
16	5.820	2.660	15.32	0.800	1.164	0.0229	0.720
17	4.680	0.500	16.88	2.600	1.544	0.0191	0.072
18	7.340	3.920	8.300	2.800	0.936	0.1000	0.288
19	5.060	1.940	3.620	1.200	0.404	0.0832	1.656
20	3.920	3.740	14.54	2.100	1.012	0.0030	0.936
21	8.480	4.820	7.520	0.900	1.468	0.0012	1.584
22	1.260	2.120	1.280	1.800	0.632	0.0017	0.360
23	10.00	0.680	20.00	2.300	0.328	0.0091	1.440
24	8.100	2.300	6.740	0.600	1.772	0.0076	0.648
25	3.160	3.200	18.44	2.500	0.480	0.0398	1.512
26	3.540	2.480	0.500	2.000	1.620	0.0014	0.864
27	10.00	4.990	0.576	2.365	0.100	0.1000	1.800
28	2.054	0.503	19.96	0.507	1.031	0.0993	0.365
29	9.417	3.653	2.808	0.928	0.383	0.0704	0.003
30	5.176	1.526	20.00	3.000	0.103	0.0010	0.585
31	10.00	4.490	15.66	1.189	2.000	0.0426	0.440
32	0.501	1.856	0.549	2.973	1.360	0.0117	1.491
33	5.859	0.555	2.095	2.209	1.991	0.0011	1.420
34	0.506	2.357	15.70	1.515	0.104	0.0044	0.002
35	4.747	3.311	2.431	0.500	0.825	0.0119	1.800
36	5.067	4.462	8.021	1.600	0.501	0.0998	0.893
37	9.856	0.789	19.19	1.485	0.707	0.0025	1.662
38	4.500	5.000	15.27	2.999	1.759	0.0654	0.246
39	3.483	4.999	4.751	0.500	0.344	0.0219	1.080
40	1.691	4.086	15.19	2.663	0.335	0.0010	1.796
41	7.652	0.942	0.517	0.776	0.911	0.0440	0.124
42	7.989	0.505	4.107	2.780	0.129	0.0713	0.846
43	10.00	2.882	17.46	0.501	1.304	0.0015	1.279
44	8.837	2.096	12.13	2.088	0.496	0.0206	1.795
45	0.591	4.435	19.99	1.012	1.637	0.0061	0.739
46	1.218	3.185	6.600	2.995	1.625	0.0998	0.000
47	9.158	4.942	9.151	2.579	1.052	0.0019	0.594
48	3.182	3.956	7.989	2.203	0.100	0.0106	0.316
49	3.307	0.784	11.89	1.164	1.402	0.0921	0.623
50	2.729	4.976	19.82	1.742	1.997	0.0034	0.097
51	7.315	3.266	19.99	1.213	0.213	0.0015	1.096

Table 2. List of experiments. Symbols according to Appendix A.

Case	KE ergs/cm^3	MMT Sv	NHT PW	CONV	TEMP °C	DOWN
1	0.450	10.30	0.231	19	3.96	3038
2	1.423	24.83	0.731	65	5.02	2534
4	0.934	28.42	0.764	388	4.38	2258
5	0.589	8.88	0.265	424	3.73	2299
6	0.671	24.37	0.638	559	4.52	2532
7	0.299	19.38	0.494	5	4.06	2456
8	0.385	12.06	0.350	4	3.68	2031
9	1.104	11.78	0.437	147	3.55	2034
10	0.958	20.10	0.612	235	4.17	2219
11	0.723	13.77	0.462	422	3.97	2211
12	1.182	23.54	0.784	389	4.79	2479
13	0.293	11.34	0.310	375	3.95	2662
14	1.070	28.51	0.776	519	5.07	2563
16	0.883	22.63	0.619	52	4.46	2406
17	0.310	21.04	0.505	354	4.30	2532
20	0.581	16.75	0.512	319	4.11	2438
21	1.489	25.04	0.784	855	5.47	2592
22	0.174	8.95	0.244	337	3.42	2259
24	0.975	28.60	0.715	404	4.81	2692
25	0.886	14.58	0.495	1	3.80	2120
26	0.444	16.40	0.467	665	4.44	2492
28	0.327	14.06	0.320	38	3.88	2256
30	0.579	16.45	0.579	948	4.33	2334
32	0.484	9.08	0.233	131	3.63	2511
33	0.829	22.79	0.627	1276	5.19	2536
35	2.166	22.25	0.580	161	4.63	2369
37	1.895	24.11	0.889	1237	5.39	2236
40	0.933	9.54	0.397	566	3.83	2343
41	1.023	26.81	0.661	53	4.41	2113
43	1.736	28.56	0.837	1012	5.59	2609
44	1.435	24.31	0.823	62	4.53	2328
45	0.230	8.12	0.190	82	3.56	2730
47	0.791	25.74	0.775	554	4.87	2679
49	0.441	17.42	0.437	38	4.24	2373
50	0.145	14.04	0.392	187	3.98	2814
51	1.309	18.18	0.765	702	4.87	2474

Table 3. Model output.

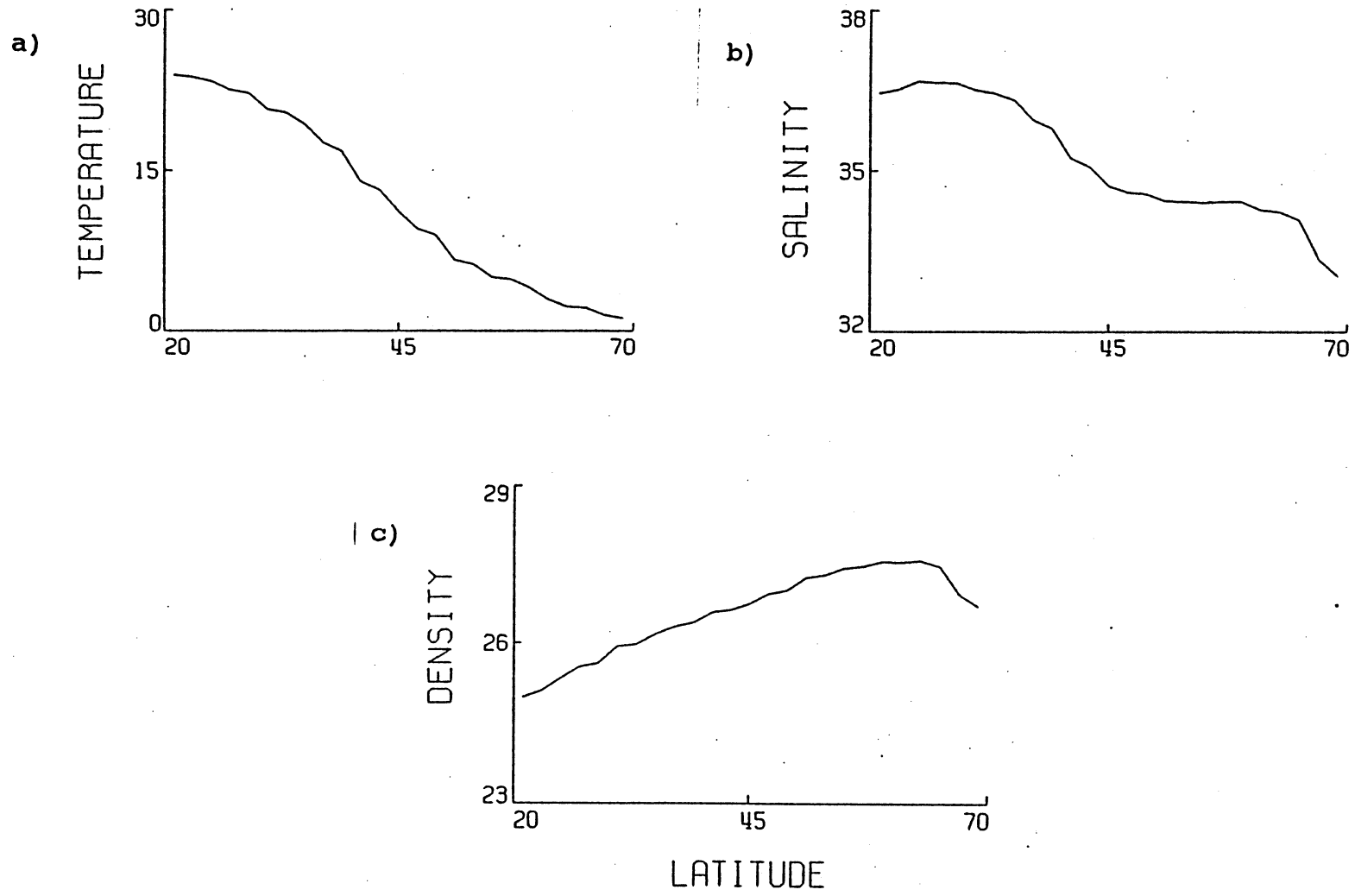
a)
TEMPERATURE
30
15
0
20
45
70
b)
SALINITY
38
35
32
20
45
70
c)
DENSITY
29
26
23
20
45
70
LATITUDE

Cross Validation Predictions Versus True Values

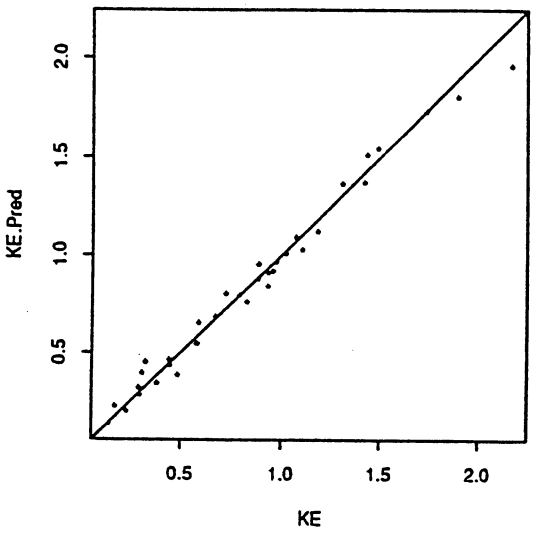

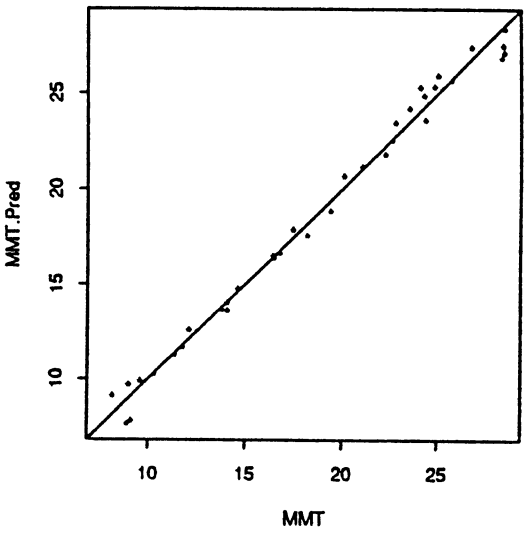

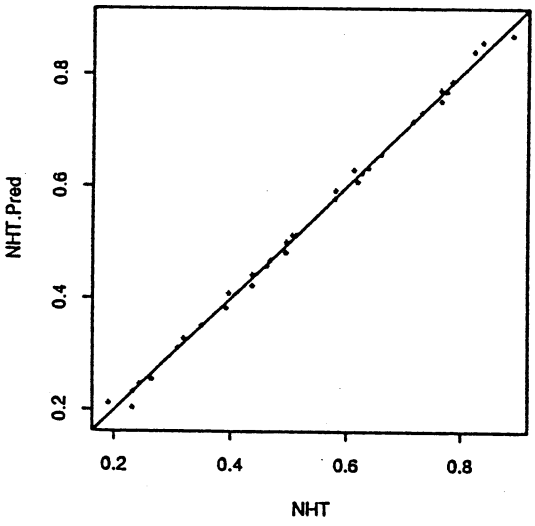

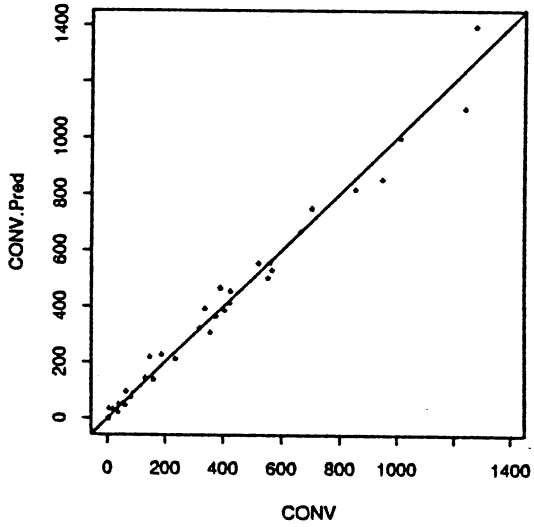

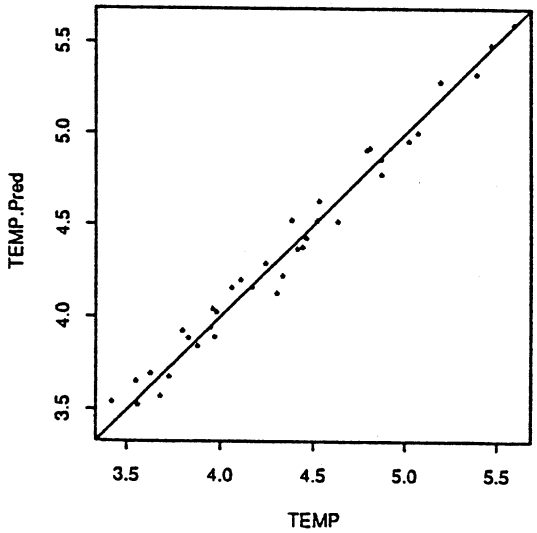

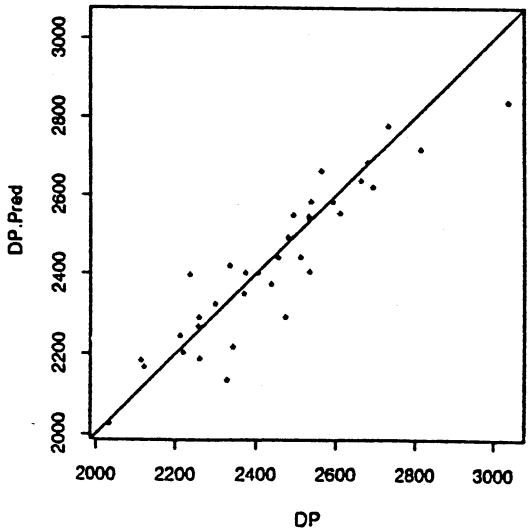

Main Effects for KE

KE(DIA) : 31.1%

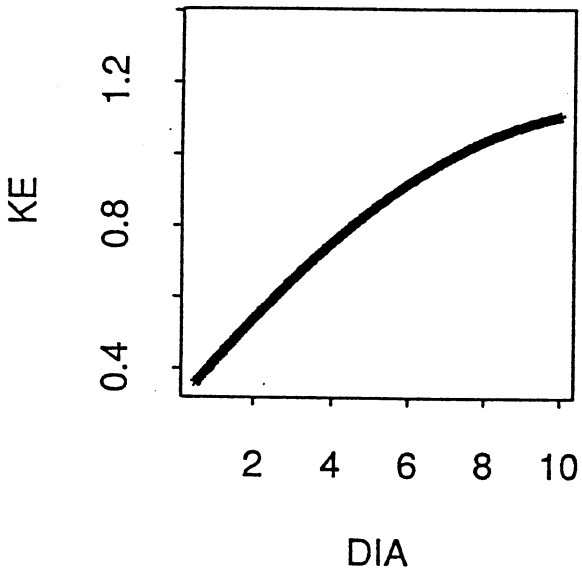

KE(HORVIS) : 13.0%

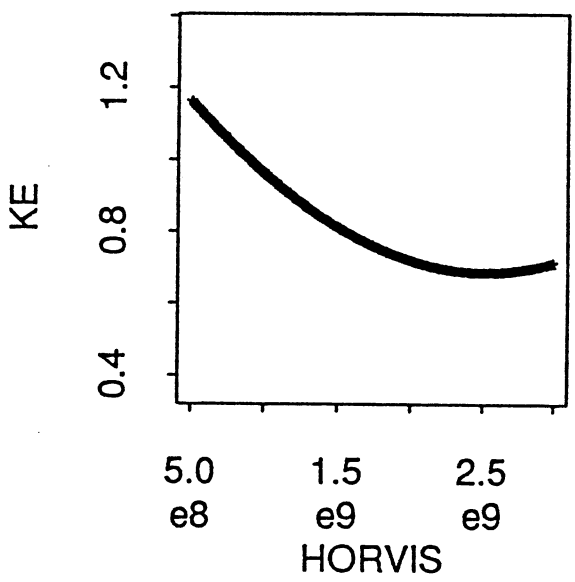

KE(BACK) : 4.6%

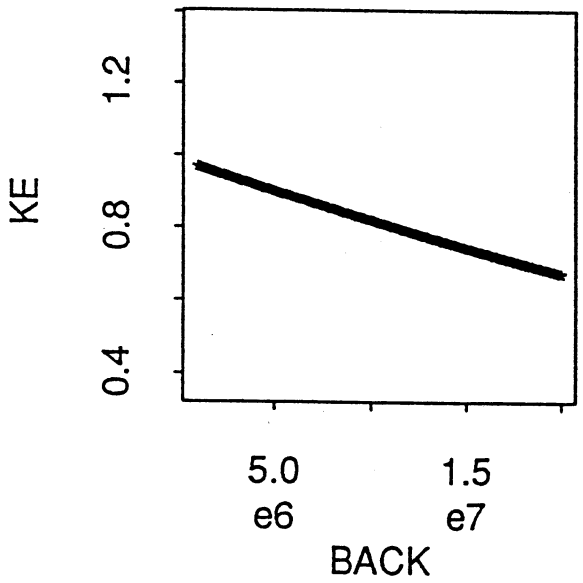

KE(WIND) : 44.4%

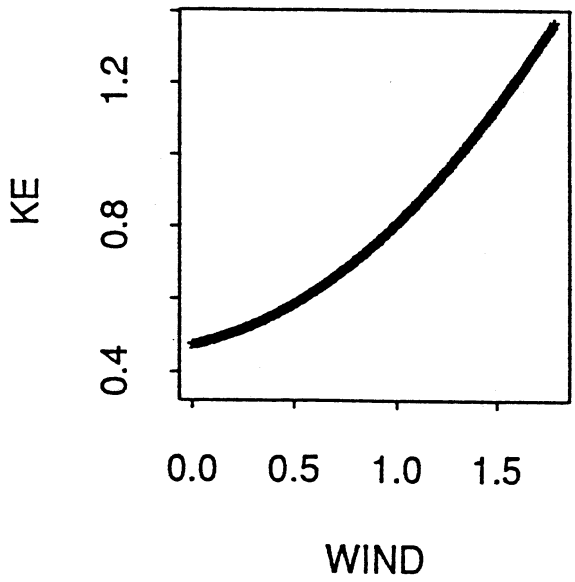

Main Effects for MMT

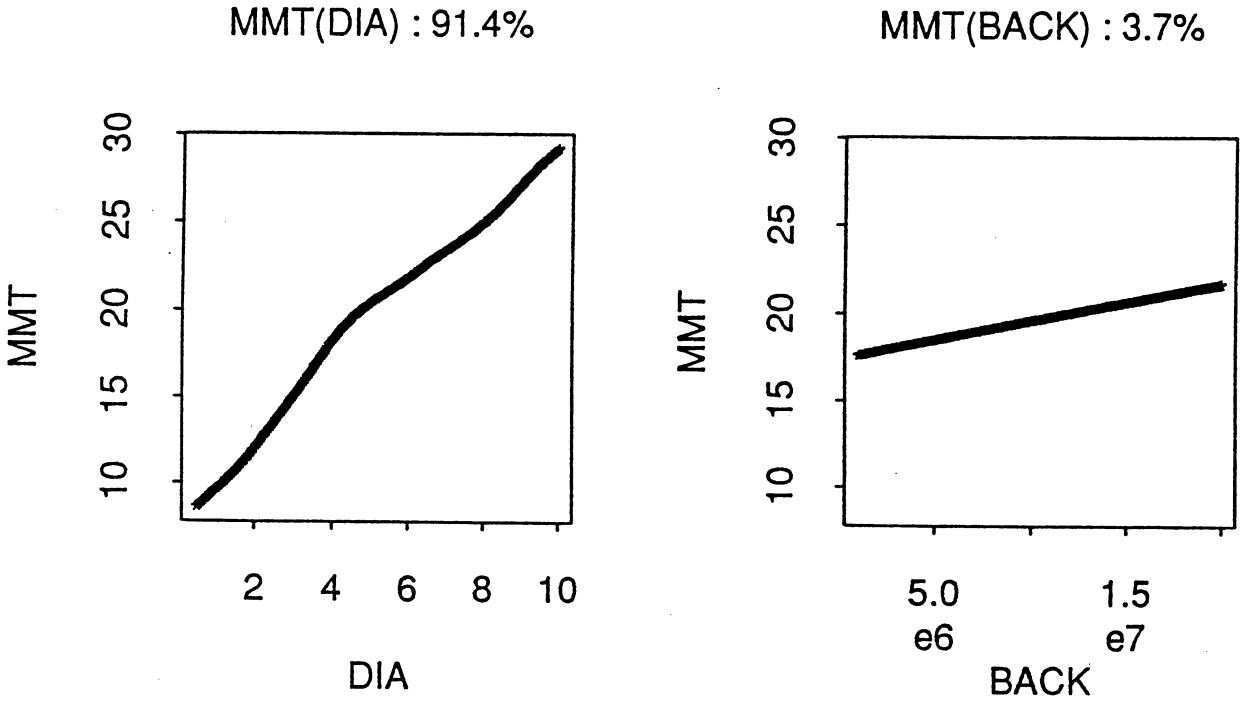

Main Effects for NHT

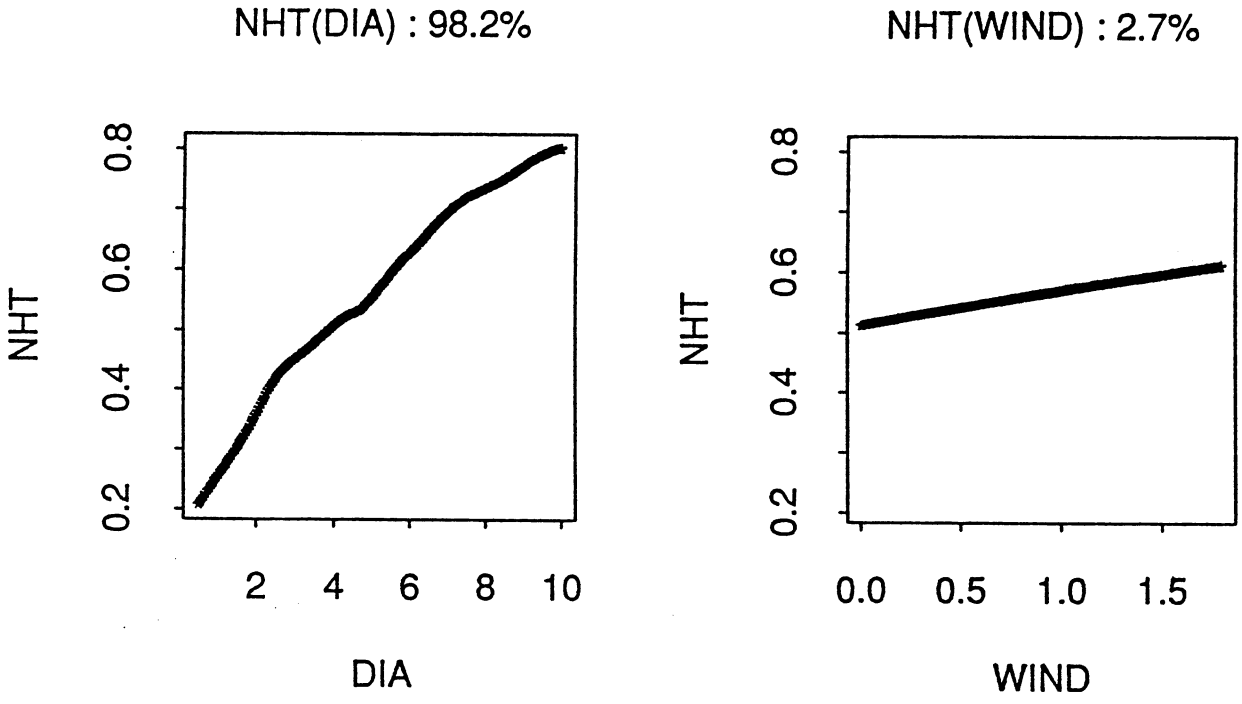

Main Effects for CONV

CONV(ISO) : 10.3%

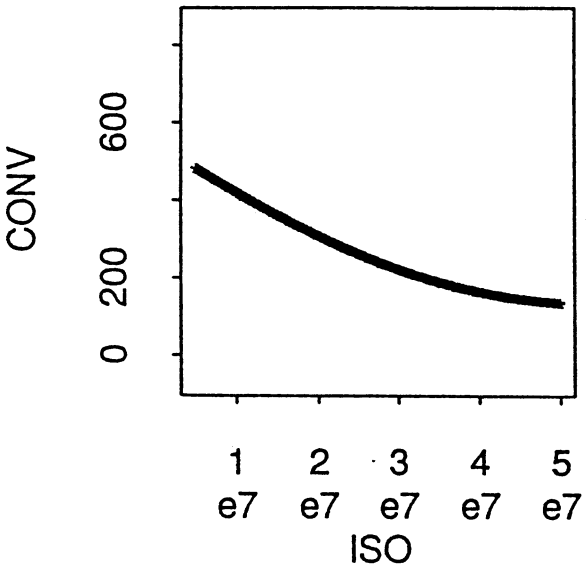

CONV(BACK) : 2.6%

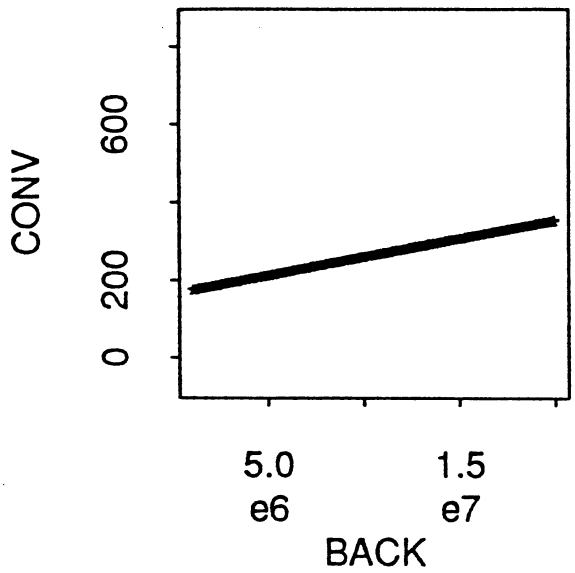

CONV(MAXSLP) : 72.7%

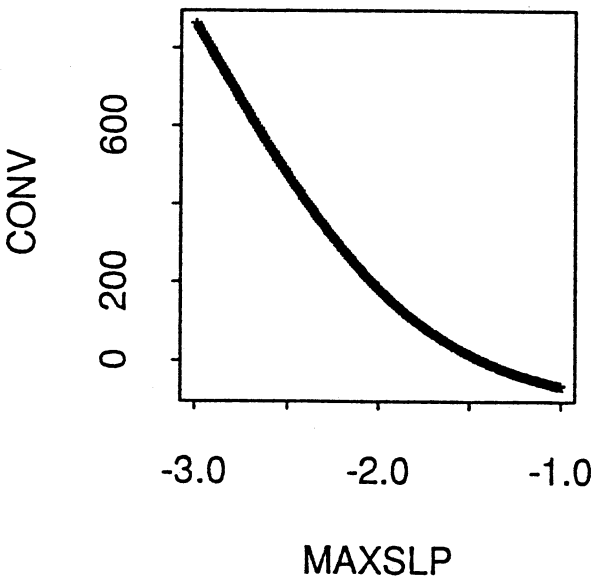

Main Effects for DP

DP(DIA) : 3.1%

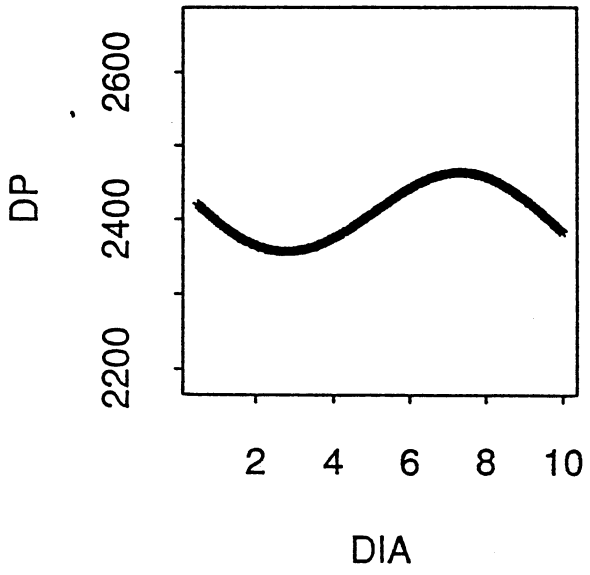

DP(BACK) : 59.8%

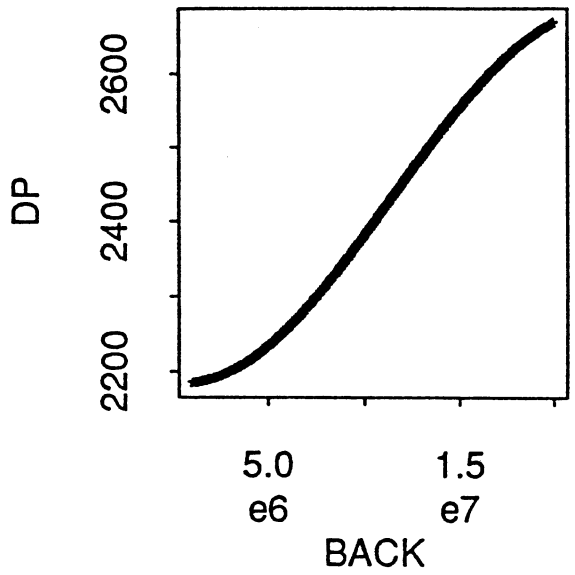

DP(MAXSLP) : 13.1%

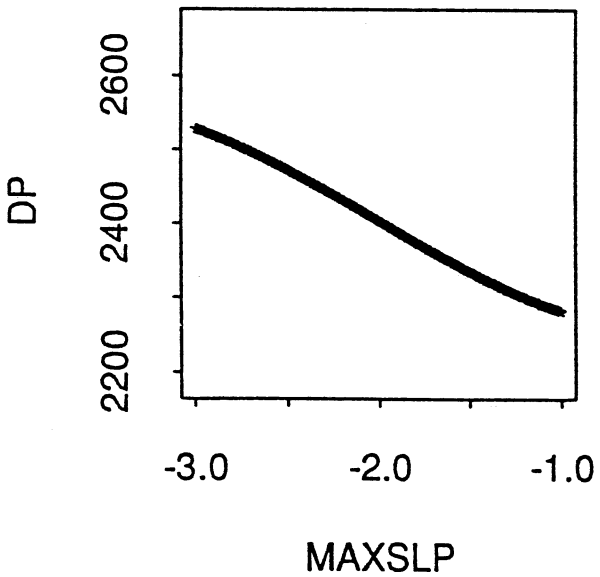

Main Effects for TEMP

TEMP(DIA) : 68.7%

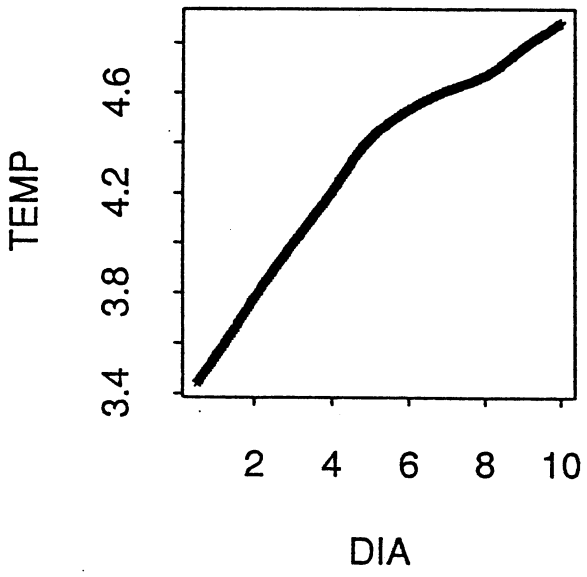

TEMP(BACK) : 15.8%

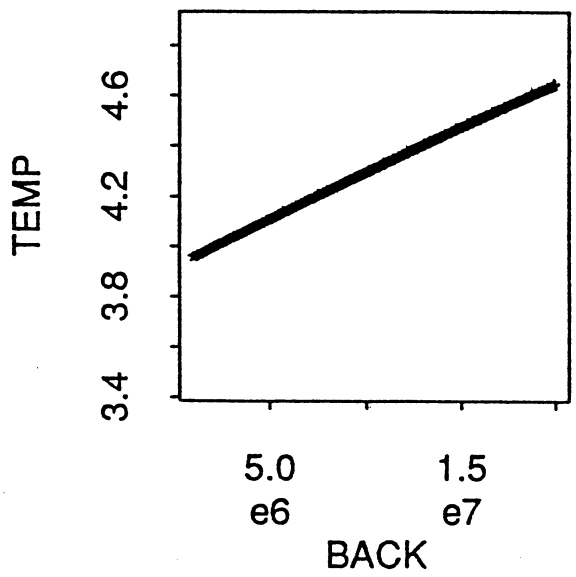

TEMP(MAXSLP) : 4.5%

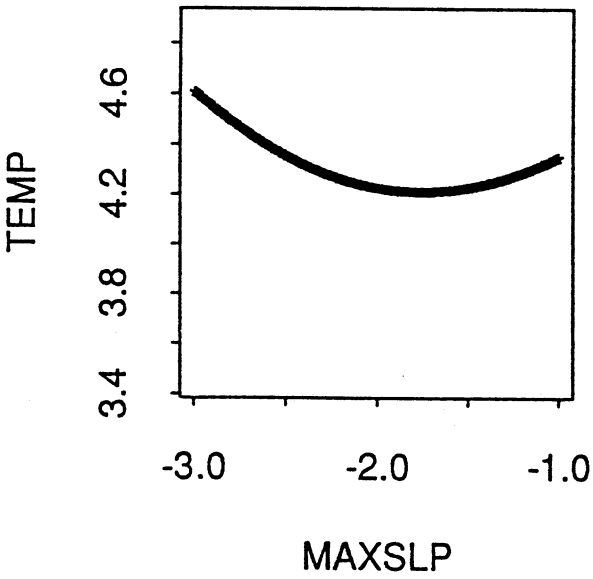

TEMP(WIND) : 7.3%